

A study of the nuclear structure of light nuclei at the Electron-Ion Collider

Niseem Magdy,^{1,*} Mariam Hegazy,² Aliaa Rafaat,³ Wenliang Li,^{4,†} Abhay Deshpande,^{5,6,4}
A. M. H. Abdelhady,² A.Y.Ellithi,² Roy A. Lacey,^{7,5} and Zhoudunming Tu^{6,‡}

¹Department of Physics, University of Tennessee, Knoxville, TN, 37996, USA

²Department of Physics, Faculty of Science, Cairo University, Giza 12613, Egypt

³Department of Physics, The American University in Cairo, New Cairo 11835, Egypt

⁴Center for Frontiers in Nuclear Science at SBU, Stony Brook, NY 11794, USA

⁵Department of Physics, Stony Brook University, Stony Brook, NY 11794, USA

⁶Department of Physics, Brookhaven National Laboratory, Upton, New York 11973, USA

⁷Department of Chemistry, Stony Brook University, Stony Brook, NY 11794, USA

The substructure of atomic nuclei resulting from the clustering of nucleons is crucial for understanding nuclear structure and dynamics. Various cluster configurations can emerge depending on excitation energy, the number and types of core clusters, and the presence of excess neutrons. Despite the prevalence of tightly bound cluster formations in low-lying states, understanding the correlation between clusters and their formation mechanisms remains incomplete. This exploring study investigates nuclear clustering at the Electron-Ion Collider (EIC) using simulations based on the modified BeAGLE model. By simulating collisions involving $e+{}^9\text{Be}$, $e+{}^{12}\text{C}$, and $e+{}^{16}\text{O}$ nuclei, we find that the average energy of particles $\langle E \rangle$ and the system size ratios of particles at forward rapidity exhibit sensitivity to alpha clustering and its various configurations. These findings offer valuable insights into the dynamics of nuclear clustering and its implications for future studies at the EIC.

PACS numbers:

I. INTRODUCTION

Exploring the complex interactions among nucleons within atomic nuclei remains a central challenge in nuclear physics, driving research into diverse theoretical frameworks and experimental methodologies. Of particular interest is the inquiry into cluster structures within nuclear matter, which sheds light on the intricate interplay between nucleons and the emergence of distinctive structural motifs [1–7].

Cluster structures arise when nucleons aggregate into discernible groups, presenting diverse shapes and sizes. The concept of alpha particles as elemental building blocks, originating from Wefelmeier’s pioneering work in 1937 [8], has been foundational in studying light nuclei. Ikeda’s seminal work in 1968 [9] introduced the Ikeda diagram, enriching our comprehension by predicting various cluster structures within light nuclei. Notably, mean-field effects have been found insufficient to disrupt cluster formation [10].

Alpha clustering, commonly observed in excited states of light nuclei, extends to ground states, particularly in nuclei situated distant from the stability line [11]. These nuclei are often depicted as quasi-molecular entities composed of clusters [12–17] as illustrated in Fig. 3. Notably, extensive research over the past five decades has focused on elucidating 3-alpha and 4-alpha clustered structures in ${}^{12}\text{C}$ and ${}^{16}\text{O}$, respectively [18–21]. Antisymmetrized

Molecular Dynamics (AMD) calculations have also provided insight, indicating that states above the decay threshold (such as the Hoyle band) exhibit a pronounced cluster structure. However, it’s becoming evident that even within the ground state, the influence of cluster structures may not be negligible [22, 23]. Nuclear lattice simulations have similarly addressed this phenomenon, further highlighting the potential significance of cluster structures in the ground state [24].

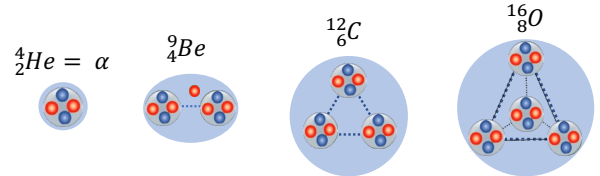


Fig. 1: Schematic illustrations of α clustering in atomic nuclei, panel (a) ${}^4\text{He}=\alpha$ particle, (b) ${}^8\text{Be}$, (c) ${}^{12}\text{C}$ and (d) ${}^{16}\text{O}$. The blue areas represent the space existence of clusters in the nucleus.

In the 2030s, the Electron-Ion Collider will provide access to nuclear-deep inelastic scattering for the first time in collider kinematics [25], providing a wealth of new opportunities to study nuclear structures. Therefore, in this study, we are raising the question, *can the future EIC provide a deep understanding of the α -clustering in the nuclei ground state and help constrain different theoretical models?* To provide an answer to such a question, we employed the BeAGLE model [26], a leading $e+A$ event generator, to study the α -clustering in light ions at the EIC. Using the BeAGLE model framework, we explored the sensitivity of the mean energy ($\langle E \rangle$) at forward rapidity to the α -clustering in light ions. A simple first

*Electronic address: niseemm@gmail.com

†Electronic address: billlee@jlab.org

‡Electronic address: zhoudunming@bnl.gov

measurement we present in this work is the mean energy $\langle E \rangle$ of the particles at forward rapidity. In $e+A$ collisions, we anticipate the particles at forward rapidity to be created in various processes, such as hard collisions, nuclear evaporation, nuclear fission, and intra-nuclear cascade. In addition, we expect the energy of those particles to depend on the impact parameter and, therefore, on the nuclear configuration [26].

Here, an important objective is to develop a more strict constraint for measuring α -clustering at the EIC using the $e+{}^9\text{Be}$, $e+{}^{12}\text{C}$, and $e+{}^{16}\text{O}$ collisions. The paper is organized as follows. Section II summarizes the theoretical model used to investigate the α -clustering effect on the mean energy of the neutrons at forward rapidity. The results from the model studies are presented in Sec. II C followed by a summary in Sec. III.

II. METHODOLOGY

The study employed version 1.03 of the Monte Carlo code "Benchmark eA Generator for LEptonproduction" (BeAGLE) [26]. BeAGLE, a versatile FORTRAN program tailored for simulating electron-nucleus (eA) interactions, served as the cornerstone of our analysis. Notably, we leveraged the GLISSANDO [27, 28] module within BeAGLE, which we updated in the current version to explore the nuclear structure effect on the $\langle E \rangle$ measured at forward rapidity.

A. The BeAGLE model

BeAGLE operates as a hybrid model, synergizing various established codes DPMJet [29], PYTHIA6 [30], PyQM [31], FLUKA [32, 33], and LHAPDF5 [34] to comprehensively describe high-energy leptonuclear scattering phenomena.

- DPMJet model defines hadron creation and interactions with the nucleus via an intra-nuclear cascade.
- PYTHIA-6 model, which gives the partonic interactions and subsequent fragmentation process.
- PyQM model provides the geometric density distribution of nucleons in a nucleus. In addition, the model executes the Salgado-Wiedemann quenching weights to represent the partonic energy loss [35].
- FLUKA model describes the decay of the excited nuclear remnant (i.e., nucleon and light ion evaporation, nuclear fission, Fermi breakup of the decay fragments, and photon emission de-excitation).
- LHAPDF5 model and FLUKA model define the high-energy lepto-nuclear scattering.

In addition, BeAGLE provides steering, multi-nucleon scattering (shadowing), and an improved description of the Fermi momentum distributions of nucleons in the nuclei.

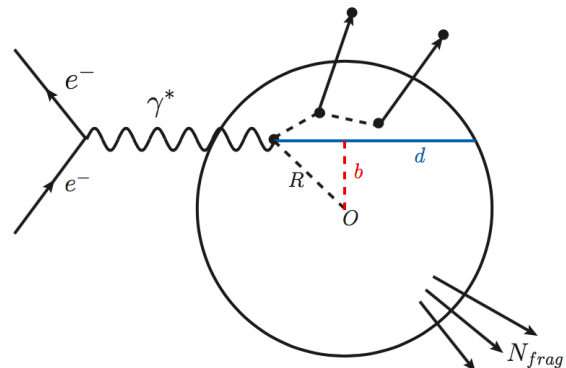


Fig. 2: Diagram illustrating geometric features of the leptonuclear scattering process in the BeAGLE model. The variable b is referred to as the impact parameter, with small values indicating “central collisions” and large values indicating “peripheral collisions.”

BeAGLE offers many options to manipulate simulation phenomena. This includes the ability to describe nuclear shadowing via various approaches, account for hadron formation time in the DPMJet intranuclear cascade, and tailor the Fermi motion of nucleons within the nucleus through different mechanisms. PyQM functionalities extend to specifying the transport coefficient \hat{q} to modulate the interaction degree between energetic partons and the nuclear environment and fine-tune details of the partonic energy loss process. The main program, DPMJet, interfaces with PYTHIA6 to handle elementary interactions and fragmentation. PyQM, in turn, manages this process directly post-elementary interactions in PYTHIA6, while DPMJet is responsible for nuclear geometry and nuclear evaporation post-fragmentation facilitated by FLUKA.

The BeAGLE model, as it currently stands, omits clustering and cluster configurations. Therefore, we adopt the α -clustering provided by the GLISSANDO model prescription [27, 28] for ${}^9\text{Be}$ (2α +neutron), ${}^{12}\text{C}$ (3α), and ${}^{16}\text{O}$ (4α) see (see Fig. 3). In the GLISSANDO model, as illustrated in Fig. 3, the centers of the clusters are separated by a distance d . The nucleons’ position in each cluster is randomly chosen according to a Gaussian distribution;

$$f_i(\vec{r}) = A e^{-\frac{3}{2} \left(\frac{\vec{r} - \vec{c}_i}{\sigma_c} \right)^2}, \quad (1)$$

where \vec{r} is the x, y and z coordinate of a nucleon, \vec{c}_i is the i^{th} cluster center, and σ_c is the RMS radius of the cluster. Then, the nucleons’ x, y, and z positions are generated successively, swapping between clusters. In the current study, the size of the α -cluster is 1.1 fm for all systems, and the distance between the centers of clusters

is chosen to be 3.6, 2.8 a.d 3.2 fm for ${}^9\text{Be}$, ${}^{12}\text{C}$, and ${}^{16}\text{O}$ respectively. Note that for ${}^9\text{Be}$, we have an extra neutron in addition to the two α clusters. The extra neutron is included via the distribution;

$$f_n(\vec{r}) = B r^2 e^{-\frac{3}{2}(\frac{r}{\sigma_n})^2}. \quad (2)$$

In addition, the centers of each nucleon pair are forbidden from being closer than the expulsion distance of 0.9 fm [36]. Finally, the obtained distributions are shifted such that their center of mass is positioned at the origin of the coordinate frame. Consequently, we get the Monte Carlo distributions with the cluster correlations included. The comparison of the nucleons' positions generated using the Woods Saxon Distribution and the α -clustering model used in this work are given in Fig. 3.

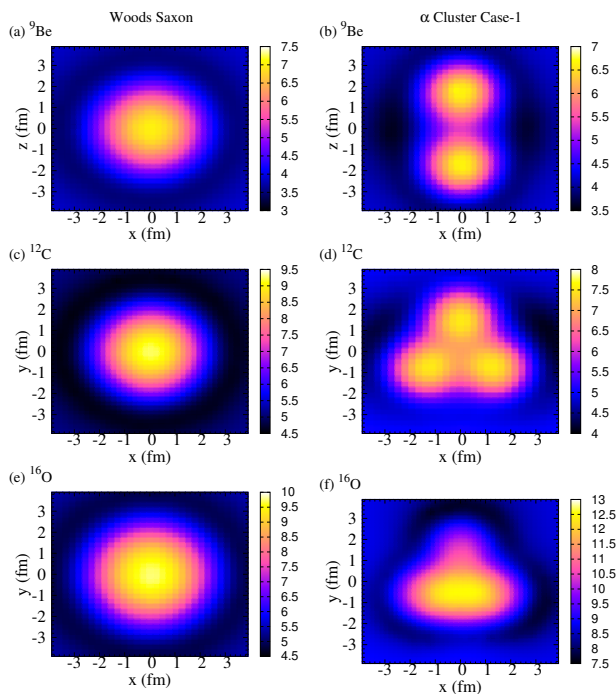


Fig. 3: Comparison of the nucleons density distribution at different positions generated using the Woods Saxon Distribution (a),(c),(e) and the α -clustering model (b),(d),(f) for ${}^8\text{Be}$, ${}^{12}\text{C}$, and ${}^{16}\text{O}$.

In the present work, nucleons in a nucleus are distributed according to four cases;

- Case-1, according to the Woods–Saxon density distribution.
- Case-2, according to our description for clustered nuclei with a dipole, trigonal planar, and tetrahedral shapes for ${}^9\text{Be}$, ${}^{12}\text{C}$ and ${}^{16}\text{O}$ respectively. In Case-2, the clustered nuclei have a fixed orientation along the z-axis.
- Case-3, same as case-2 but with random orientation.

- Case-4, according to our description for clustered nuclei with chain shape [37] for ${}^{12}\text{C}$ and ${}^{16}\text{O}$. In Case-4, the clustered nuclei have a random orientation.

B. Observable

In this work, we use the mean energy of particles ($\langle E \rangle$) at forward rapidity $4.5 < \eta < 5.9$ as our mean observable. The $\langle E \rangle$ is given as;

$$\langle E \rangle = \frac{\sum_i w_i E_i}{\sum_i w_i}, \quad (3)$$

where, the sum runs over the particle in the η acceptance between 4.5–5.9, E_i and w_i are the i^{th} particle energy and weight. For a perfect detector $w_i = 1.0$.

This work presents the results as functions in collision centrality defined via cuts over the impact parameter distribution, see 2. In e+A collisions, the impact parameter is independent of the collision kinematics and weakly depends on the final state particles [26]. Such properties complicate identifying a final state measure that can correlate strongly with the impact parameter. Consequently, finding a clever way to define centrality in the e+A collisions at the EIC is essential and will be considered in future work, see Appendix. A.

C. Results and discussion

Before delving into exploring nuclear structure studies at the forthcoming Electron-Ion Collider (EIC), we meticulously prepared the initial coordinate space for the light nuclei target, as depicted in Fig 3. Subsequently, we utilized the BeAGLE model framework to generate simulated data under standardized conditions for each collision system. Our approach began with a focused analysis of scenarios where the nuclei are oriented in fixed positions. In this context, we chose distinct spatial configurations for different nuclei. The ${}^9\text{Be}$ designed with two clusters aligned along the collision axis (z-axis). The ${}^{12}\text{C}$ was designed with three clusters situated within the plane perpendicular to the collision axis (x-y plane). The ${}^{16}\text{O}$ is created with three clusters within the x-y plane and an additional cluster along the z-axis. This preliminary investigation is directed toward ensuring the correct implementation of the initial nuclear configuration into the BeAGLE model.

Figure 4 panels (a), (b), and (c) provide a comparative analysis of the average energy ($\langle E \rangle$) of particles within the pseudorapidity range $4.6 < \eta < 5.9$ for $e+{}^9\text{Be}$, $e+{}^{12}\text{C}$, and $e+{}^{16}\text{O}$ collisions, respectively, utilizing data generated by the BeAGLE model under fixed orientation nuclei conditions. Our findings across all collision systems consistently revealed a decrease in $\langle E \rangle$ as collision centrality transitioned towards more peripheral

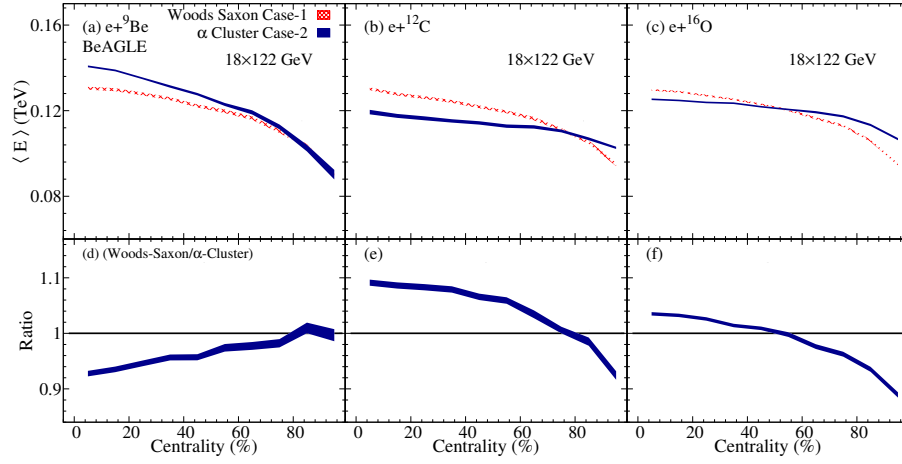


Fig. 4: The centrality dependence of the mean energy of the particles in $4.6 < \eta < 5.9$ for $e+{}^9\text{Be}$ (a), $e+{}^{12}\text{C}$ (b) and $e+{}^{16}\text{O}$ (c) from the BeAGLE model. Panels (d), (e), and (f) show the ratios between the Woods-Saxon density distribution Case-1 and α clustering with fixed orientation nuclei Case-2.

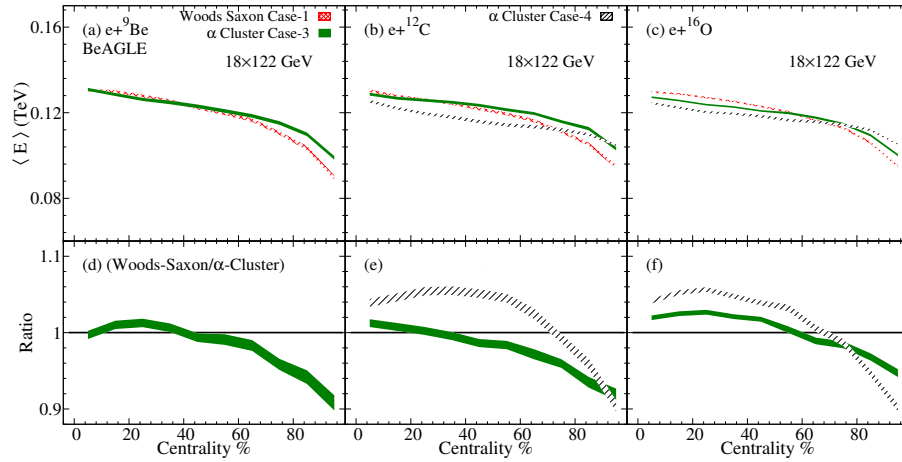


Fig. 5: Same as in Fig. 4 but for clustering with random orientation nuclei Case-3 and Case-4.

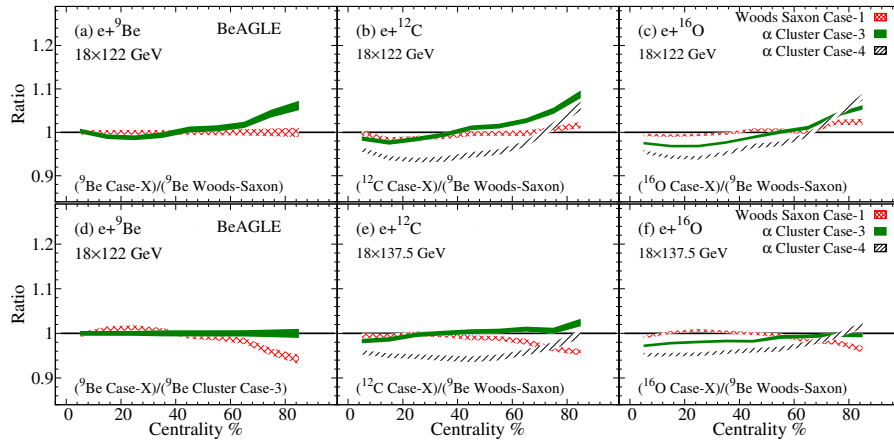


Fig. 6: The centrality dependence of the $\langle E \rangle$ ratios to the ${}^9\text{Be}$ Case-1 panels (a), (b) and (c), and to the ${}^9\text{Be}$ Case-3 panels (e), (f) and (g).

configurations. Further insights into the impact of different nuclear configurations on particle energies were gleaned by comparing $\langle E \rangle$ ratios between scenarios with Woods–Saxon density distribution (Case-1) and those with α clustering under fixed orientation nuclei conditions (Case-2), as depicted in Fig. 4 panels (d), (e), and (f). In the case of $e+{}^9\text{Be}$ collisions (panel (d)), where two alpha clusters align along the collisions axis, we observed a higher $\langle E \rangle$ for the α cluster Case-2 compared to the Woods–Saxon Case-1 in central collisions. Conversely, for $e+{}^{12}\text{C}$ collisions (panel (e)), featuring three alpha clusters within the x-y plane, there was a reduction in $\langle E \rangle$ for the α cluster Case-2 relative to the Woods–Saxon Case-1 in central to mid-central collisions. Notably, in $e+{}^{16}\text{O}$ collisions (panel (f)), characterized by three alpha clusters in the x-y plane and one cluster along the z-axis, we observed a reduction (growth) in $\langle E \rangle$ for the clustered case in central (peripheral) collisions. Our analyses underscore the sensitivity of $\langle E \rangle$ at forward rapidity to the underlying α clustering structure, as evidenced by the presented ratios. Consequently, we place greater confidence in our implementation of the ion configurations within the BeAGLE model framework.

In practice, the orientation of target nuclei cannot be fixed, necessitating a reevaluation of our analysis with nuclei orientations randomized. Similar to the methodology employed for Fig. 4, we present a comparative study in Figure. 5 panels (a), (b), and (c), illustrating the average energy ($\langle E \rangle$) of particles within the pseudorapidity range $4.6 < \eta < 5.9$ for $e+{}^9\text{Be}$, $e+{}^{12}\text{C}$, and $e+{}^{16}\text{O}$ collisions, respectively, utilizing data from the BeAGLE model. Across all scenarios, our computations consistently reveal a $\langle E \rangle$ reduction as collision centrality progresses towards more peripheral selections. The corresponding $\langle E \rangle$ ratios relative to the Woods–Saxon distribution (Case-1) are depicted in panels (d), (e), and (f) of Figure. 5. Notably, our findings demonstrate a consistent trend among the various collision systems. Specifically, we observe an increase in $\langle E \rangle$ for the clustered case in peripheral collisions, with the magnitude of this increase depending on the system size and the configuration of clusters (e.g., chain configuration). These observations underscore the sensitivity of $\langle E \rangle$ at forward rapidity to the α clustering structure and configurations, emphasizing the importance of considering nuclear structure effects in our analyses.

Furthermore, we expanded our analysis by constructing a series of ratios between (i) each system and the $e+{}^9\text{Be}$ Case-1 and (ii) each system and the $e+{}^9\text{Be}$ Case-3. These ratios offer insights into the influence of nuclear structure on energy distributions. Ideally, these ratios should approximate unity if no discernible nuclear structure is present, implying that all systems can be adequately described by a simple Woods–Saxon distribution. Conversely, deviations from unity in these ratios would suggest the presence of nuclear structure effects.

Figure 6 illustrates the dependence of the $\langle E \rangle$ ratios on the ${}^9\text{Be}$ Case-1 (panels (a), (b), and (c)) and the

${}^9\text{Be}$ Case-3 (panels (d), (e), and (f)). Our analysis revealed that for Case-1, where nuclear structure effects are absent, all ratios closely approximate unity. However, when the ratios incorporate systems with included nuclear structure, deviations from unity become apparent. These deviations underscore the sensitivity of the ratios to the presence of α clustering structure and its configurations. This observation reinforces the importance of accounting for nuclear structure effects when interpreting energy distributions in e+A collisions.

III. CONCLUSION

Using the modified BeAGLE model framework, we explored the potential of studying the effect of nuclear structure (i.e., α clustering) on the produced final state particles at forward rapidity. Our $\langle E \rangle$ results of light nuclei indicated centrality characteristic patterns that depend on the clusters' configurations and the system size. In addition, we constructed a set of ratios between different systems that deviate from unity when one or more of the systems contain nuclear structures. Our findings underscore the sensitivity of both $\langle E \rangle$ and system size ratios of particles at forward rapidity to the presence and configurations of α clustering within the nucleus. This sensitivity underscores the intricate interplay between nuclear structure and particle production dynamics in e+A collisions, emphasizing the need to consider these effects in comprehensive analyses. Consequently, our results lend credence to the proposal put forth by antisymmetrized molecular dynamics and nuclear lattice simulations regarding the potential presence of cluster structures in the ground state of light nuclei. The validation of these hypotheses at the forthcoming Electron-Ion Collider (EIC) holds promise for advancing our understanding of nuclear structure and its implications for particle production mechanisms.

Acknowledgments

This work was supported in part by funding from the Division of Nuclear Physics of the U.S. Department of Energy under Grant No. DE-FG02-96ER40982 (NM) and DE-SC0012704 (ZT). ZT acknowledge the support of the Laboratory Directed Research and Development (LDRD) 22-027 and LDRD-23-050 project. AR acknowledge the support of the American University in Cairo under the agreement Number: SSE-PHYS-A.H-FY24-RG-2023-Dec-17-14-59-41.

Appendix A: Centrality definition in e+A collisions

In prior investigation [26], it has been proposed that the energy deposited in the Zero-Degree Calorimeter (ZDC) with angular acceptance $\theta < 5.5$ rad ($\eta > 6.0$) can

be used to define the centrality in e+A collisions. Figure 7 presents the correlations between energy deposited in the ZDC and the impact parameter in panel (a). Such correlations indicated that the ZDC deposited energy increases weakly as the b decreases. Figure 7 panel (b) shows the b distributions in central (0%–1%) and peripheral (60%–100%) collisions. The distributions are normalized by the total number of events. A weak difference is observed between central and peripheral collisions. Such observation suggests that using the ZDC energy as an experimental handle on the collision geometry is complicated.

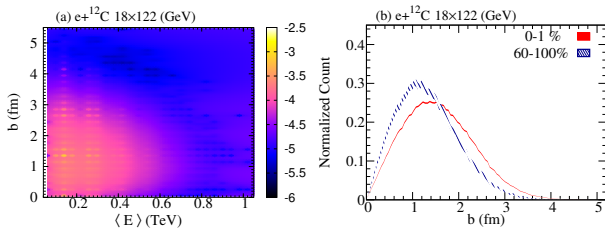


Fig. 7: The correlations between energy deposited in the Zero-Degree Calorimeter (ZDC) and the impact parameter (b) is shown in panel (a). The comparison of b distributions in central and peripheral collisions as determined by Zero-Degree Calorimeter energy cuts are presented in panel (b).

-
- [1] M. Freer, H. Horiuchi, Y. Kanada-En'yo, D. Lee, and U.-G. Meißner, *Rev. Mod. Phys.* **90**, 035004 (2018), 1705.06192.
- [2] S. A. AFZAL, A. A. Z. AHMAD, and S. ALI, *Rev. Mod. Phys.* **41**, 247 (1969).
- [3] H. Feldmeier and J. Schnack, *Rev. Mod. Phys.* **72**, 655 (2000), cond-mat/0001207.
- [4] D. Lee, *Prog. Part. Nucl. Phys.* **63**, 117 (2009), 0804.3501.
- [5] R. Roth, T. Neff, and H. Feldmeier, *Prog. Part. Nucl. Phys.* **65**, 50 (2010), 1003.3624.
- [6] P. Schuck, Y. Funaki, H. Horiuchi, G. Röpke, A. Tohsaki, and T. Yamada, *Phys. Scripta* **91**, 123001 (2016), 1702.02191.
- [7] A. Tohsaki, H. Horiuchi, P. Schuck, and G. Roepke, *Rev. Mod. Phys.* **89**, 011002 (2017), 1702.04591.
- [8] W. Wefelmeier, *Zeitschrift für Physik* **107**, 332 (1937).
- [9] K. Ikeda, N. Takigawa, and H. Horiuchi, *Progress of Theoretical Physics Supplement* **E68**, 464 (1968), ISSN 0375-9687, <https://academic.oup.com/ptps/article-pdf/doi/10.1143/PTPS.E68.464/5216547/E68-464.pdf>, URL <https://doi.org/10.1143/PTPS.E68.464>.
- [10] W. B. He, Y. G. Ma, X. G. Cao, X. Z. Cai, and G. Q. Zhang, *Phys. Rev. C* **94**, 014301 (2016), URL <https://link.aps.org/doi/10.1103/PhysRevC.94.014301>.
- [11] *Physics Reports* **432**, 43 (2006), ISSN 0370-1573, URL <https://www.sciencedirect.com/science/article/pii/S0370157306002626>.
- [12] J. Hiura and I. Shimodaya, *Progress of Theoretical Physics* **30**, 585 (1963), ISSN 0033-068X, <https://academic.oup.com/ptp/article-pdf/30/5/585/5236544/30-5-585.pdf>, URL <https://doi.org/10.1143/PTP.30.585>.
- [13] K. Ikeda, N. Takigawa, and H. Horiuchi, *Progress of Theoretical Physics Supplement* **68**, 464 (1968).
- [14] G. Avakov, E. Dolinsky, and V. Turovtsev, *Nuclear Physics A* **196**, 529 (1972), ISSN 0375-9474, URL <https://www.sciencedirect.com/science/article/pii/0375947472907919>.
- [15] W. Wefelmeier, *Zeitschrift für Physik* **107**, 332 (1937).
- [16] J. A. Wheeler, *Physical Review* **52**, 1083 (1937).
- [17] H. Morinaga, *Physical Review* **101**, 254 (1956).
- [18] C. W. Cook, W. A. Fowler, C. C. Lauritsen, and T. Lauritsen, *Phys. Rev.* **107**, 508 (1957), URL <https://link.aps.org/doi/10.1103/PhysRev.107.508>.
- [19] Y. Fujiwara, H. Horiuchi, K. Ikeda, M. Kamimura, K. Katō, Y. Suzuki, and E. Uegaki, *Progress of Theoretical Physics Supplement* **68**, 29 (1980), ISSN 0375-9687, <https://academic.oup.com/ptps/article-pdf/doi/10.1143/PTPS.68.29/5434765/68-29.pdf>, URL <https://doi.org/10.1143/PTPS.68.29>.
- [20] M. Freer and H. O. U. Fynbo, *Prog. Part. Nucl. Phys.* **78**, 1 (2014).
- [21] P. Schuck, *AIP Conf. Proc.* **2038**, 020002 (2018), 1811.11580.
- [22] Y. Kanada-En'yo, *Prog. Theor. Phys.* **117**, 655 (2007),

- [Erratum: Prog.Theor.Phys. 121, 895–895 (2009)], nucl-th/0605047.
- [23] K. Kravvaris and A. Volya, Phys. Rev. Lett. **119**, 062501 (2017).
- [24] E. Epelbaum, H. Krebs, T. A. Lahde, D. Lee, and U.-G. Meissner, Phys. Rev. Lett. **109**, 252501 (2012), 1208.1328.
- [25] R. Abdul Khalek et al., Nucl. Phys. A **1026**, 122447 (2022), 2103.05419.
- [26] W. Chang, E.-C. Aschenauer, M. D. Baker, A. Jentsch, J.-H. Lee, Z. Tu, Z. Yin, and L. Zheng, Phys. Rev. D **106**, 012007 (2022), 2204.11998.
- [27] P. Bożek, W. Broniowski, M. Rybczyński, and G. Stefanek, Computer Physics Communications **245**, 106850 (2019), ISSN 0010-4655, URL <https://www.sciencedirect.com/science/article/pii/S0010465519302279>.
- [28] M. Rybczyński, M. Piotrowska, and W. Broniowski, Phys. Rev. C **97**, 034912 (2018), 1711.00438.
- [29] S. Roesler, R. Engel, and J. Ranft, in *International Conference on Advanced Monte Carlo for Radiation Physics, Particle Transport Simulation and Applications (MC 2000)* (2000), pp. 1033–1038, hep-ph/0012252.
- [30] T. Sjostrand, S. Mrenna, and P. Z. Skands, JHEP **05**, 026 (2006), hep-ph/0603175.
- [31] R. Dupré, Ph.D. thesis, Lyon, IPN (2011).
- [32] T. T. Böhlen, F. Cerutti, M. P. W. Chin, A. Fassò, A. Ferrari, P. G. Ortega, A. Mairani, P. R. Sala, G. Smirnov, and V. Vlachoudis, Nucl. Data Sheets **120**, 211 (2014).
- [33] A. Ferrari, P. R. Sala, A. Fassò, and J. Ranft (2005).
- [34] M. R. Whalley, D. Bourilkov, and R. C. Group, in *HERA and the LHC: A Workshop on the Implications of HERA and LHC Physics (Startup Meeting, CERN, 26-27 March 2004; Midterm Meeting, CERN, 11-13 October 2004)* (2005), pp. 575–581, hep-ph/0508110.
- [35] C. Salgado and U. A. Wiedemann, Phys. Rev. D **68**, 014008 (2003), hep-ph/0302184.
- [36] W. Broniowski and M. Rybczynski, Phys. Rev. C **81**, 064909 (2010), 1003.1088.
- [37] B. S. Huang, Y. G. Ma, and W. B. He, Phys. Rev. C **95**, 034606 (2017), 1803.07972.